
**AFRL-AFOSR-VA-TR-2021-111**

# Feasibility of quantum computing with electrons trapped in a Paul trap

**Haeffner, Hartmut**
**REGENTS OF THE UNIVERSITY OF CALIFORNIA**
**2150 SHATTUCK AVE RM 313**
**BERKELEY, CA,**
**US**

**08/25/2021**
**Final Technical Report**



Air Force Research Laboratory
Air Force Office of Scientific Research
Arlington, Virginia 22203
Air Force Materiel Command

# REPORT DOCUMENTATION PAGE

*Form Approved*
*OMB No. 0704-0188*



| **1. REPORT DATE** *(DD-MM-YYYY)* | **2. REPORT TYPE** | **3. DATES COVERED** *(From - To)* |
|---|---|---|
| 25-08-2021 | Final | 01 Jul 2020 - 30 Jun 2021 |

**4. TITLE AND SUBTITLE**
Feasibility of quantum computing with electrons trapped in a Paul trap

**5a. CONTRACT NUMBER**

**5b. GRANT NUMBER**
FA9550-20-1-0162

**5c. PROGRAM ELEMENT NUMBER**
61102F

**6. AUTHOR(S)**
Hartmut Haeffner

**5d. PROJECT NUMBER**

**5e. TASK NUMBER**

**5f. WORK UNIT NUMBER**

**7. PERFORMING ORGANIZATION NAME(S) AND ADDRESS(ES)**
REGENTS OF THE UNIVERSITY OF CALIFORNIA
2150 SHATTUCK AVE RM 313
BERKELEY, CA
US

**8. PERFORMING ORGANIZATION REPORT NUMBER**

**9. SPONSORING/MONITORING AGENCY NAME(S) AND ADDRESS(ES)**
AF Office of Scientific Research
875 N. Randolph St. Room 3112
Arlington, VA 22203

**10. SPONSOR/MONITOR'S ACRONYM(S)**
AFRL/AFOSR RTB1

**11. SPONSOR/MONITOR'S REPORT NUMBER(S)**
AFRL-AFOSR-VA-TR-2021-111

**12. DISTRIBUTION/AVAILABILITY STATEMENT**
A Distribution Unlimited: PB Public Release

**13. SUPPLEMENTARY NOTES**

**14. ABSTRACT**
We studied the feasibility of a novel architecture for quantum computing which uses trapped electrons as carriers of quantum information. In comparison to current state-of-the-art technologies, electrons have the potential of storing quantum information for longer times than solid-state systems and allow for reducing the technological overhead of atomic systems. In view of this, we demonstrated trapping of electrons in a 3-layer PCB Paul trap. Fur-ther, we conducted extensive theoretical, numerical and design studies on how a small electron quantum computer might look like. We ï¬•nd that building on the technology of generating AC-magnetic ï¬•eld gradients, one should be able to initialize, control and read out quantum information encoded in spin degree-of-freedom of single electrons with high precision. Further our numerical studies show that two-qubit gates with error rates of less than one error per 10,000 operations are within reach of current technology

**15. SUBJECT TERMS**

| **16. SECURITY CLASSIFICATION OF:** | | | **17. LIMITATION OF ABSTRACT** | **18. NUMBER OF PAGES** | **19a. NAME OF RESPONSIBLE PERSON** |
|---|---|---|---|---|---|
| **a. REPORT** | **b. ABSTRACT** | **c. THIS PAGE** | | | GRACE METCALFE |
| U | U | U | UU | 19 | **19b. TELEPHONE NUMBER** *(Include area code)* (703) 696-9740 |

# Final report: feasibility study of electron based quantum computing

Qian Yu, Alberto M. Alonso, Jackie Caminiti, Kayla J. Rodriguez, Madhav Dhital, Boerge Hemmerling, Hartmut Häffner

July 29, 2021

**Abstract:** We studied the feasibility of a novel architecture for quantum computing which uses trapped electrons as carriers of quantum information. In comparison to current state-of-the-art technologies, electrons have the potential of storing quantum information for longer times than solid-state systems and allow for reducing the technological overhead of atomic systems. In view of this, we demonstrated trapping of electrons in a 3-layer PCB Paul trap. Further, we conducted extensive theoretical, numerical and design studies on how a small electron quantum computer might look like. We find that building on the technology of generating AC-magnetic field gradients, one should be able to initialize, control and read out quantum information encoded in spin degree-of-freedom of single electrons with high precision. Further our numerical studies show that two-qubit gates with error rates of less than one error per 10,000 operations are within reach of current technology.

**Motivation:** The general idea of our approach is replacing the ions in a trapped-ion quantum computer with electrons. Electrons are attractive for quantum computing primarily because they are extremely light, have a simple two-level spin structure, and can be manipulated with well-established microwave technology, eliminating the need for qubit control optics. The mass reduction of four orders of magnitude, as compared to trapped ions, increases the motional frequencies of the particle in the trapping potential, thereby considerably increasing the speed for shuttling and other motion-based operations. The small mass of the electron is also favorable for increasing two-qubit gate speed. Additionally, the electron's ideal two-level structure removes complications of traditional atomic and solid-state qubits such as leakage of quantum information from the computational subspace, thus making high-fidelity operations easier and simplifying quantum error correction [1]. Further, the electron's spin degree of freedom can be initialized, coherently controlled, and measured using microwaves, making all-electronic control feasible and thus removing some of the optical engineering challenges required to build large scale quantum information processing devices with trapped ions.

Quantum computing with electrons in Paul traps has been proposed and discussed by us and others in Refs. [2–4]. During the review period of this pro-

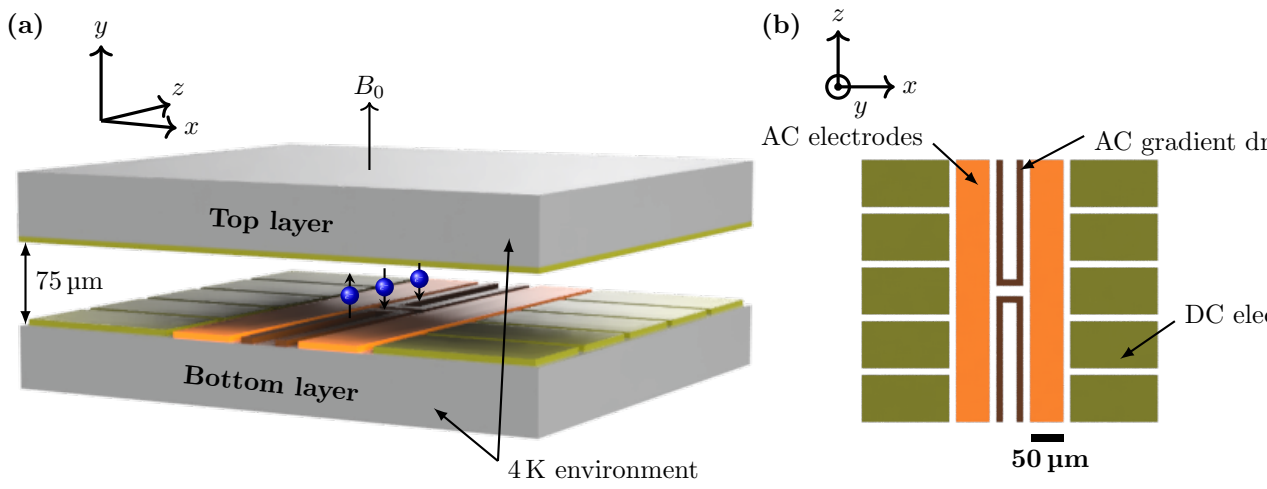


Figure 1: **(a)** Our preliminary trap design provides a framework for analyzing the feasibility of trapped electron quantum computing, such as estimating sources of decoherence and heat load management. The trap consists of two substrates separated by 75 µm: the bottom substrate houses the trap, including the electrodes for the power intensive AC drive for trapping as well as for the magnetic field gradient. The separation of high power and low power elements should allow us to cool the top layer, and especially the cooling resonator, significantly below 4 K if needed. **(b)** Top view of the bottom substrate.

posal, we already took the first step towards this goal by trapping and detecting electrons in a room-temperature 3-layer-PCB Paul trap [5]. Thus, and because of the restrictions imposed by the pandemic, our work focused on surveying and studying challenges of trapped-electron quantum computing. We decided to investigate those by designing a prototype providing a framework to analyse the expected performance as well as technological requirements. Similar to nearly all other quantum computing technologies, we anticipate that multi-qubit operations will be the most critical challenge. Thus, we carried out detailed simulations of quantum gate fidelities to determine dominant error sources.

# 1 Prototype

The prototype, residing in a cryogenic environment, is sketched in Fig. 1. We chose a surface trap design with a top layer 75 µm above the bottom layer to provide a large trap depth. Applying $U_0 \cos(\omega_{\mathrm{ac}} t)$ to the AC electrodes on the bottom layer with $U_0 = 17\,\mathrm{V}$ and drive frequency of $\omega_{\mathrm{ac}} = 2\pi \times 10.6\,\mathrm{GHz}$ yields transverse secular frequencies $\omega_{\mathrm{t}}$ of $2\pi \times 2\,\mathrm{GHz}$ and an axial trap frequency $\omega_{\mathrm{a}} = 2\pi \times 300\,\mathrm{MHz}$. Using the pseudo potential approximation we

find a trap depth of approximately 110 meV while numerical simulation of electron trajectories without the pseudo-potential approximation shows substantial losses for electrons with an initial energy of 6 meV (see Appendix D). The minimum of the trapping potential resides at 28 µm above the bottom layer. The average micro-motion amplitude of a thermalized electron at 4 K $x_{\mathrm{MM}} = \frac{q}{2} x_{\mathrm{t}} = 0.2\,\mu\mathrm{m}$, where $q = 0.53$ is the stability parameter in the Matthieu equation, and $x_{\mathrm{t}} = \sqrt{\frac{2k_{\mathrm{B}}T}{m_e \omega_t^2}} \approx 0.9\,\mu\mathrm{m}$ is the amplitude of the transverse secular motion. Low-energy electrons can be introduced to the trap by, for example, photoionizing a thermal atomic beam near the trap center [5].

The electron motion is damped and detected by coupling the induced image current to a resonant cryogenic tank circuit, which creates a voltage opposing the electron motion that is dissipated over the effective resistance of the circuit until the thermal energy of the electron is equivalent to the circuit temperature. The quantum information is assumed to be stored in superpositions of the $|\uparrow\rangle$ and $|\downarrow\rangle$ states of the electron. We assume that a homogeneous magnetic field $B_0 = 3.6\,\mathrm{mT}$ splits the degeneracy of the two spin states, leading to a frequency difference of $\omega_{\mathrm{qubit}} = 2\pi \times 100\,\mathrm{MHz}$ between both logical eigenstates.

The electron qubits will be controlled with the help of the two "hairpin" electrodes between the AC electrodes. The spin direction of the electrons can be detected by using a magnetic field gradient to apply a spin-dependent force and measuring an image charge in one of the electrodes [3]. When carrying currents of opposite helicity, these hairpin electrodes create a magnetic field gradient that can be used to drive multi-qubit gates. Reversing the helicity produces a homogeneous magnetic field along the trap axis that can drive single-qubit gates.

## 1.1 Cooling of electrons

One of the main requirements for the envisioned electron quantum computing platform is trapping electrons and cooling them to low temperatures to minimize the extent of their thermal motion, thus allowing for a non-destructive spin state readout. The electron motion can be damped by coupling the image current induced by the electron motion to a high-impedance cryogenic tank circuit, as demonstrated in Penning trap experiments [6]. The damping occurs because the image current induced in the tank circuit is dissipated by the circuit's resistance, creating a voltage at the trap electrodes that opposes the electron motion until the induced current is of similar magnitude as the thermal (Johnson) current fluctuations in the circuit.

The induced current is $I = ev/d_{\mathrm{eff}}$, where $v$ is the velocity of the electron with charge $e$ and $d_{\mathrm{eff}}$ describes the effective distance of the electrode structure [6, 7]. For the geometry discussed here, with the electron trapped 28 µm above the bottom layer, we find $d_{\mathrm{eff}} = 79\,\mu\mathrm{m}$. The cooling time constant for the principal transverse mode can be derived by considering the electron as a circuit element

$$\tau = \frac{m_e}{e^2} \frac{d_{\mathrm{eff}}^2}{\mathrm{Re}(Z)} \approx 2.8\ \mu s\,. \tag{1}$$

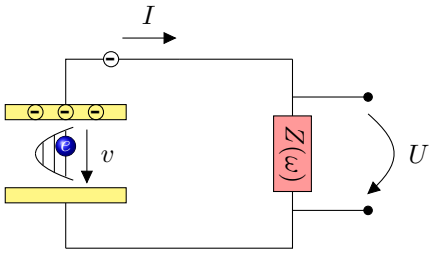


Figure 2: The trapped electron induces an image current in the trap electrodes, which is measured and dissipated via the impedance of an attached tank circuit.

Here, $m_e$ is the electron mass, and $Z = Q\sqrt{L/C}$ the on-resonance impedance of the attached circuit. Assuming that the pick-up electrode is attached to a tank circuit with a moderate quality factor of $Q = 1,000$, a capacitance of 1 pF, a resonant frequency of $2\pi \times 2\,\mathrm{GHz}$, and an inductance of 6 nH results in an on-resonance impedance of $\mathrm{Re}(Z) = 80\,\mathrm{k\Omega}$. Inserting this into Eq. (1), we find a cooling time constant of 2.8 µs.

In equilibrium, the energy of the cooled mode will be that of the (electronic) temperature of the tank circuit, i.e. $\langle E \rangle = \hbar\omega_\mathrm{t}(\bar{n} + 1/2) = k_\mathrm{B}T_\mathrm{t}$. Assuming 2 GHz for one of the transverse modes and $T_\mathrm{t} = 4\,\mathrm{K}$, the average motional excitation will be $\bar{n} \approx 40$.

We assume the transverse mode to be cooled with this protocol as it has the largest trap frequency and hence the smallest achievable harmonic oscillator quantum number for a given temperature. The low frequency axial mode (∼300 MHz) can be cooled by coupling it to the transverse mode. Such a coupling is common practice for electrons and ions in Penning traps [7] and has been demonstrated for ions in a Paul trap [8]. To achieve this coupling, we use specific voltage configurations on the electrodes to generate a quadrupole field with projection overlap on both modes and oscillating at the difference frequency. This leads to an exchange in quanta between the two motional modes. Assuming that we hold the high-frequency transverse mode at 4 K, the low-frequency axial mode will be cooled to a temperature reduced by the frequency ratio, $T_\mathrm{a} = T_\mathrm{t} \cdot \omega_\mathrm{a}/\omega_\mathrm{t} = 0.6\,\mathrm{K}$. Scaling our results from Ref. [8], we expect coupling times between the two motional modes of below 1 $\mu$s.

In contrast to laser cooling, resistive cooling does not affect the internal state of the qubit. As a consequence, the electrons can be cooled while keeping the qubits coherent, and no sympathetic coolant-particles are needed. In fact, the cooling does not need to be turned off for most of the time; only during multi-qubit gates where the motion is used as a bus, as well as during the spin-motion conversion process for detection, must the cooling be switched off. We also note that efficient cooling takes place only if the electron motion is on-resonance. Thus, we can adjust the cooling time constant by changing the trapping potential.

## 1.2 Spin readout and initialization of electrons

The spin direction $\{\uparrow,\downarrow\}$ can be read-out by first coupling the spin to the electron motion and then measuring the phase of the motion as discussed in Ref. [3]. We updated those calculations based on the numbers provided by the prototype.

In order to couple the spin direction to the motion, one can apply a magnetic field gradient oscillating at the axial motional frequency. As the direction of the force due to the magnetic field gradient depends on the spin direction, this creates a state of the form $P_\uparrow |\uparrow\rangle |-\alpha\rangle + P_\downarrow |\downarrow\rangle |\alpha\rangle$. The measurement result is encoded in the phase of $|\alpha\rangle$, and thus the critical requirement is to maintain the coherence of this state. Therefore, it is important to create the displaced state faster than the motional dephasing time. Because of this, one of the limiting factors is the strength of the magnetic field gradient. We calculate that passing 1 A of current through the hairpin wires in Fig. 1 will create a gradient of 140 T/m. Oscillating this current at the axial motional frequency of the electrons for 16 µs maps the spin direction to the motion with a fidelity of 99.7 %, assuming an axial mode temperature of 0.6 K, cooled via parametric coupling as described in Sec. 1.1. To increase the amplitude of the image current further to a readily measurable size, electric forces can be used to parametrically amplify the coherent state $|\alpha\rangle$ by modulating the trapping voltages at twice the trap frequency [9, 10].

As mentioned, it is critical to conserve phase coherence. Therefore, it is necessary to consider the harmonicity of the axial trapping potential created by the DC electrodes in Fig. 1. Experimentally one tunes the DC voltages to minimize the anharmonicities. Expanding the optimized trap potential into the Taylor series $V(z) = V(0)(1 + c_2 z^2 + c_4 z^4 + c_6 z^6)$ and $c_2 = 1(\mu\text{m})^{-2}$, we find coefficients $c_4 = 10^{-7}(\mu\text{m})^{-4}$ and $c_6 = -2 \times 10^{-9}(\mu\text{m})^{-6}$, while odd and higher even order terms are negligible and assuming a typical 16-bit DAC voltage uncertainty of 200 µV for each trapping voltage. From this we find the trap frequency uncertainty as $\Delta\omega_\text{a}/\omega_\text{a} \approx (3A^2 c_4/4 + 15A^4 c_6/16)/c_2$ , where $A$ is the amplitude of the motion. To excite the motion above the Johnson noise, the amplitude must exceed $A > 1.6\,\mu\text{m}$. At this amplitude, the relative frequency shift due to the trap anharmonicity would be only $2 \times 10^{-7}$, corresponding to an absolute shift of the resonance frequency of 60 Hz, which is negligible on the considered timescale of 16 µs.

The current induced by the motion of the electron produces a voltage drop across the tank circuit that can be picked up with a Johnson-noise limited amplifier. The phase of the electron motion is then encoded in the phase of the amplified voltage.

Electronic detection of electrons is standard in Penning traps [7, 11–13]. In Paul traps, however, the strong trap drive of $\sim$ 100 V may saturate the amplifiers, requiring careful filtering (see Appendix B). We note that this may turn out to be one of the most challenging steps towards a small scale trapped-electron quantum computer.

With state read-out in place, we can initialize the spin of electrons by first measuring it and then flipping it conditioned on the measurement result. If the

electron is found in the state we would like to initialize it in, nothing is done. If it is in the other state, we perform a $\pi$-pulse using a microwave field, i.e. a single-qubit gate.

### 1.3 Quantum gates with electrons

Single-qubit gates can be performed by using microwave pulses near the Zeeman resonance, similarly to how error rates of $10^{-5}$ have been achieved for ions[14].

For the analysis of two-qubit gates, the Mølmer-Sørensen gate [15, 16] and its controlled phase gate ($\sigma_z \otimes \sigma_z$) variant [17] are considered. While typically performed using optical-frequency radiation, it can also be implemented using oscillating magnetic field gradients [18–21]. The general idea is that a force oscillating nearly resonant with a mode frequency of the two-electron crystal excites the motion if the force on the individual electrons has the correct symmetry. For the phase gate variant, a gradient oscillating at $\omega_\mathrm{a} \pm \delta$ with $\delta \ll \omega_\mathrm{a}$ excites the center-of-mass motion of the electron crystal if the electrons are in the same spin-state, i.e. $|\uparrow\uparrow\rangle$ or $|\downarrow\downarrow\rangle$. If the electrons are in the $|\uparrow\downarrow\rangle$ or $|\downarrow\uparrow\rangle$ state, the net force vanishes and the electron-COM motion is not excited. The corresponding Hamiltonian in the interaction picture is given by [16, 17]

$$\hat{H} = \mu_\mathrm{B} \frac{dB}{dz} z_0 (\hat{I} \otimes \hat{\sigma}_z + \hat{\sigma}_z \otimes \hat{I})(\hat{a} e^{-i\delta t} + \hat{a}^\dagger e^{i\delta t}), \tag{2}$$

where $\hat{a}$ is the motional mode lowering operator, $\frac{dB}{dz}$ is the strength of the magnetic field gradient, $z_0 = \sqrt{\hbar/2m_e\omega_\mathrm{a}}$ the harmonic oscillator length of the axial COM mode, $\mu_\mathrm{B}$ the Bohr magneton and $\sigma_z$ is the Pauli operator. Because of the detuning $\delta$ of the force, the motion returns for all four logical eigenstates into its initial state after the gate time $t_\mathrm{gate} = 2\pi/\delta$, enclosing an area in phase space. The two-electron state acquires a geometrical phase, which corresponds to the area enclosed, and that is correlated with the electron's spin state. For our parameters, the anticipated gate time for a two-qubit phase gate is about 2 µs.

For simplicity, we discussed the $\sigma_z \otimes \sigma_z$ gate, but $\sigma_x \otimes \sigma_x$ gates may offer certain advantages, as the drive is not near the motional frequency thereby suppressing unwanted excitation via residual electric fields. Such variants have been implemented using ions [18] with Bell state fidelities $F = \mathrm{Tr}(\rho_\mathrm{exp}\rho_\mathrm{Bell})$ reaching 99.7% [22], limited by motional heating and trap frequency instabilities, and 99.9% [23], limited mainly by motional dephasing.

## 2 Error sources of two-qubit gates

High-fidelity gate operations are crucial for achieving fault-tolerant quantum computing. We analyzed the most important sources of gate infidelities for electron qubits in this configuration. Figure 3 shows an overview of the Bell-state infidelities $(1-F)$ due to the most relevant decoherence sources (see Appendix C for details). Many of these error sources change slowly compared to the gate

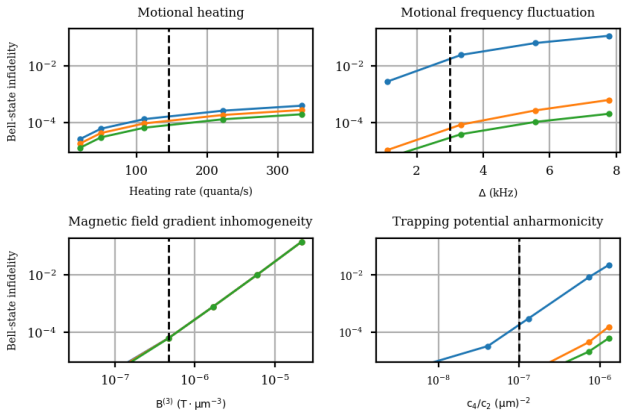


Figure 3: Numerical simulation (QuTip [**johansson2012**]) of various error sources for an electron two-qubit gate. Blue, orange and green curves correspond to Walsh 0 modulation, Walsh 1 modulation, and Walsh 3 modulation, respectively. For the magnetic field gradient inhomogeneity simulation, the three traces for different Walsh modulations overlap. To allow for an easy comparison, the $y$-axis scaling is held constant. Black dashed lines indicate our anticipated magnitude of the different error terms. Based on these error estimates, we estimate that the contribution to the Bell state infidelity is limited to $10^{-4}$ for all parameter range.

time and can be considered quasi-static. This opens up the possibility of using dynamical decoupling sequences (for example, Walsh modulation) as used in state-of-the-art trapped-ion experiments [22–27].

## 2.1 Motional heating

One of the dominant sources of error is motional heating due to surface electric field noise. The motional heating rate is proportional to the electric-field spectral noise density $S(\omega_\mathrm{a})$ [28, 29]

$$\dot{n} = \frac{e^2}{4m_e\hbar\omega_\mathrm{a}} S(\omega_\mathrm{a})\,. \tag{3}$$

For a 28-$\mu$m ion-electrode distance, $S(\omega_\mathrm{a})$ near 1 MHz is expected to be around $10^{-12}\,\mathrm{V^2m^2/Hz}$ at cryogenic temperatures [28]. This corresponds to a heating rate of $\dot{n}_\mathrm{Ca} = 100\,\mathrm{quanta/s}$ at $\omega_\mathrm{a}^\mathrm{Ca} = 2\pi \times 1\,\mathrm{MHz}$ for $\mathrm{Ca}^+$ ions. In order to extrapolate to GHz frequencies, we assume that the spectral noise density follows a power law $S(\omega_\mathrm{a}) \propto 1/\omega_a^\gamma$. For ion traps, values of $\gamma$ ranging from 1 to 1.5 have been found [29–32]. Taking into account the light mass of electrons and an axial frequency of $\omega_\mathrm{a} = 2\pi \times 300\,\mathrm{MHz}$, the expected motional heating

rate for electrons is

$$\dot{n}_{\mathrm{e}} = \frac{m_{\mathrm{Ca}}}{m_{\mathrm{e}}} \left( \frac{\omega_{\mathrm{a}}^{\mathrm{Ca}}}{\omega_{\mathrm{a}}} \right)^{1+\gamma} \dot{n}_{\mathrm{Ca}} \,, \tag{4}$$

For niobium traps at cryogenic temperatures, an exponent $\gamma = 1.3$ has been found [31], leading to an estimate for the heating rate of 14 quanta/s, which corresponds to a limit of the motional coherence time of 70 ms. Because of the uncertainties of extrapolation over two orders of magnitude in frequency, we conservatively assume a heating rate of 140 quanta/s, which corresponds to a simulated Bell-state infidelity of about $8.8 \times 10^{-5}$. For the transverse modes near 2 GHz, motional heating should be reduced by approximately two orders of magnitude to order 1 quanta/s. In addition, milling the surface with noble-gas ions may reduce electric field noise at cryogenic temperature further if this becomes an issue [31].

## 2.2 Trap frequency instabilities

Fluctuations of the trap frequency are caused by voltage noise, finite temperature in combination with anharmonic potentials, as well as surface electric field noise. Trap frequency fluctuations lead to a fluctuating detuning of the drive frequency from the motional sidebands at $\omega_{\mathrm{a}}$, thereby inducing errors.

Formally, we distinguish between fast noise (dephasing) and slow noise (trap frequency fluctuations). The reason is that slow fluctuations can be mitigated effectively using Walsh sequences [25, 33–35]. Fast noise, on the other hand, cannot be easily mitigated other than by speeding up the quantum gates or by performing more loops in phase space.

Frequency fluctuations due to noise of the voltages applied to the electrodes are expected to be slow when low-pass filtered. Typical voltage sources provide voltage stabilities on the order of $10^{-5}$, corresponding to a motional frequency fluctuation $\Delta = 2\pi \times 3$ kHz. Consequently, one can suppress the Bell-state error to below $10^{-4}$ by doing Walsh modulations.

Finite temperatures lead to trap frequency fluctuations due to the trap potential anharmonicities. Since motional heating is small as compared to the gate times, this noise is also slow and can be taken care of by using Walsh modulations.

The quadrupole component of the surface electric field noise introduces noise to the quadrupole trapping potential, thereby causing fluctuations of the trap frequency. This noise component is related to the surface electric field noise as $S_{\mathrm{Q}}(\omega_{\mathrm{a}}) = \frac{15}{4d^2} S(\omega_{\mathrm{a}})$, where $d$ is the electron-electrode distance, and exhibits a $1/f^{\alpha}$ [36] characteristics with frequency scaling exponent $\alpha \gtrsim 1$, consisting of both fast and slow noise component. Ref. [36] estimates that at $d \approx 25$ $\mu$m the integrated impact of quadrupole noise on the Bell-state fidelities is similar to that of motional heating. However, since the bulk electric field noise has a $1/f$ scaling, it can be reduced by Walsh modulations.

In order to estimate the size of the fast noise, we draw on the insights of a recent ion trap experiment where its impact has been estimated to contribute

$6 \times 10^{-4}$ to the Bell-state infidelity [10, 23]. The gate time in these experiments was with many hundred microseconds more than two orders of magnitude slower than what we expect for electrons. Thus, we expect that a significant amount of the fast noise observed in the ion trap experiments is actually slow in the context of electron quantum computing and can be removed with Walsh modulation. Assuming a $1/f$ characteristic, the remainder of the noise leads to a dephasing rate of $\Gamma = 2\pi \times 1.8 \times 10^{-3}$ Hz, which corresponds to a Bell-state infidelity of $2 \times 10^{-6}$.

## 2.3 Inhomogeneity of the magnetic field gradient

The motional amplitude of trapped electrons at 4K is on the order of 1 $\mu$m compared to nanometers for ions. As a result, the electron experiences a variation of the force over the extent of its wavefunction, due to any inhomogeneity of the magnetic field gradient. Thus, for electron qubits, the homogeneity of the applied microwave radiation in combination with the finite electron temperature is relevant.

To estimate the effect of any inhomogeneity, we do a Taylor expansion of the magnetic field gradient. Due to symmetry, the contribution of the first order term cancels over the extent of the electron. The second order term, on the other hand, introduces a loss of fidelity due to a non-cancelling force. Using the hairpin design shown in Fig. 1, we find $2 \times 10^{-7}$ T/$\mu$m$^2$ for the quadratic order in $\nabla B$ (corresponding to the third order expansion coefficient $B^{(3)} = 5 \times 10^{-7}\,\mathrm{T}/\mu\mathrm{m}^3$ for the leading order $z^3$ in the magnetic field), which causes an infidelity of $6 \times 10^{-5}$. Finally, we note that this effect can be reduced by reducing the temperature of the electrons as discussed in Appendix A.

## 2.4 Anharmonicity of the trapping potentials

The effect of the temperature on the center-of-mass mode frequency is given solely by the anharmonicity of the trapping potential itself. As discussed in Section 1.2, with the optimized trap potential up to the fourth order $V(z) = V(0)(1 + c_2 z^2 + c_4 z^4)$, we find $c_4/c_2 = 10^{-7}\,(\mu\mathrm{m})^{-2}$, which corresponds to only very small contributions to the Bell-state infidelity and is on the order of $10^{-6}$ or below for Walsh modulations (see Fig. 3). We note that a more comprehensive analysis including all three spatial coordinates is underway by Dietrich Leibfried (NIST) as, for instance, terms of the form $x^2 z^2$ also lead to changes of the axial trap frequency due to finite temperature, in this case the $x$-direction.

## 2.5 Qubit decoherence

The coherence of the electron spin is fully dominated by the magnetic field noise. Using magnetic shielding, coherence times of 300 ms and 2 s with a spin-echo have been observed for Zeeman qubits in ions [37]. We expect a similar performance for electron qubits. The greatly reduced optical overhead requirements for electron qubits as compared to the experiment in Ref. [37] will allow for more

efficient magnetic shielding, leading to expected spin-coherence times in excess of 1 s. This corresponds to only small contributions to Bell-state infidelities on the order of $5 \times 10^{-6}$.

| | Motional heating | Motional frequency fluctuation | Motional dephasing | Magnetic field gradient inhomogeneity | Trapping potential anharmonicity | Qubit decoherenc |
|---|---|---|---|---|---|---|
| Magnitude | 140 q/s | 3 kHz | $1.8 \times 10^{-3}$ Hz | $5 \times 10^{-7}$ T/$\mu$m$^3$ | $10^{-7}$ $\mu$m$^{-2}$ | 1 s |
| Infidelity | $8.8 \times 10^{-5}$ | $3.3 \times 10^{-5}$ | $2 \times 10^{-6}$ | $6 \times 10^{-5}$ | $1.7 \times 10^{-6}$ | $5 \times 10^{-6}$ |

Table 1: Estimates for the contribution of various error sources with Walsh 3 modulation.

### 2.6 Summary of decoherence sources

In summary, we find that the largest source of infidelities will likely be magnetic field gradient inhomogeneities and motional heating, both expected to lead to errors smaller than $10^{-4}$ as shown in Table 1. While these infidelities meet the error correction threshold, they can be improved further. For instance, ion milling may reduce motional heating [31] and thus suppress one of the largest error sources. Another path towards reducing motional heating would be to increase the electron-electrode distance. However, this will compromise the speed of operation and achievable motional frequencies. Yet another way to reduce errors is to cool the electrons substantially below 4 K with a dilution refrigerator, as discussed in Appendix A.

## 3 Modularization and Qubit Addressing

A modular approach is preferred for constructing a large-scale quantum computer, and the most promising strategy for scaling is adapting the quantum charge-coupled device (QCCD) architecture from trapped ions [38, 39]. Combining two-qubit gates with fast shuttling, we imagine entangling two electrons at specific sites in the QCCD device. These processing sites, with current-carrying wires providing the necessary magnetic-field gradient, would be on the order of 200 $\mu$m long to allow for high-fidelity qubit addressing. The storage regions could be much more densely packed, in principle, making use of three dimensions with packing densities of up to 1 electron/(5 $\mu$m)$^3$. Electrons can be shuttled between these two types of regions in a conveyor-belt fashion, and junctions connect different processing and storage units with each other on a 2D-grid to create large entangled states.

Since the trap frequencies for electrons are a factor of 300 larger than those of trapped ions, we expect that electron transport and the speed-limiting operations such as splitting and merging of the electron crystals can be carried out faster than on equivalent trapped-ions QCCD architecture. Diabatic transport

of ions over 370 $\mu$m in a multi-zone linear Paul trap on time scales on the order of 10 µs has been demonstrated [40]. In comparison, for electrons, where trap frequencies are on the order of 1 GHz, we expect that we could transport electrons over 100 $\mu$m within 10 ns, since the oscillation period is inversely proportional to the axial trap frequency. For time-critical splitting and merging operations, even for trapped ions in large ion traps with electrode-ion distances on the order of 200 $\mu$m, the corresponding time scales are 50 $\mu$s [40, 41]. The preparation times are limited by the strength of the applied octupole potential, which for small traps can be significantly larger than what has been assumed in Ref. [41]. Thus, we expect that electron crystals can be split and merged on a 100 ns timescale, which is an order of magnitude faster than the anticipated gate time on the order of 1 µs.

To build a modular electron quantum computer, coupling of remote electron qubits could be engineered with a high-impedance co-planar waveguide that distributes image currents between distant sites. In Ref. [2], we estimate such a coupling between two electrons to be on the order of 100 kHz, which is a significant improvement over current implementations of remote entanglement in trapped ion systems [42, 43].

To carry out single- and multi-qubit operations on electrons, one can use the features of the QCCD architecture. For single-qubit operations, the electrons will be spatially separated on the order of 100 µm and a magnetic field gradient of 0.36 T/m is introduced to separate the electronic transitions in frequency space by 1 MHz. Assuming a Rabi frequency of 1 MHz on the target electron qubit while suppressing the drive on the other electron by two orders of magnitudes with compensation fields from additional current-carrying wires, the residual excitation is order $10^{-4}$.

For multi-qubit gates, shuttling and splitting operations on electron crystals can be used to isolate a selected pair of electrons in a region where a localized magnetic field gradient can be applied to perform gates.

In conclusion, the discussed strategy opens a path towards fault-tolerant operation of an electron quantum computing platform.

# 4 Conclusion and outlook

In summary, we have conducted a feasibility study of trapped-electron quantum information processing technology, and have discussed the experimental steps and potential challenges towards building such a device, including experimental schemes for trapping, cooling, electronic detection, spin readout and quantum gates of electrons.

Numerical simulations of quantum gates with electron qubits show that the largest sources of infidelities will likely be magnetic field gradient inhomogeneities and motional heating, both expected to lead to Bell-state preparation infidelities below $10^{-4}$. This meets the error correction threshold, and can be improved further by ion milling or cooling electrons to lower temperatures. This system can be scaled up and modularized by adapting the QCCD architecture

similarly to trapped ion system, allowing for single-qubit addressing and participation control for multi-qubit operations. Therefore, the trapped-electron technology proposed here meets all five DiVincenzo criteria [44] for the physical realization of a quantum computer and operates at a fault-tolerant threshold.

In addition to applications to quantum information processing, the development of techniques to trap cold electrons in Paul traps may also directly impact other disciplines, such as plasma physics through the study of small cold plasma [**twedt2012**] and electron-positron interactions [45], by using cold electrons for high-resolution imaging [46], or to serve as sensitive detectors of charges – including millicharged dark matter [47]. The techniques developed here could also aid in the search for physics beyond the standard model through the preparation of cold positrons in a Paul trap for use in creating large amounts of anti-hydrogen [48].

# A Thermal loads on cryogenic trap

The most dominant heat source for the cryogenic electron trap in Fig. 1 is Joule heating from the current-carrying wires. External black-body radiation can be effectively shielded and almost completely suppressed because the operation of the electron trap requires only very minimal optical access.

Assuming AC-current carrying wires of $5 \times 10\,\mu m^2$ and a length of $175\,\mu m$ operating with a duty cycle of $\approx$ 10%, the estimated heat load is $\approx 350\,\mu W$ per 1 A of current for copper with a specific resistance of $\approx 1 n\Omega m$ at 4 K. This heat load can be easily mitigated by providing a sufficiently large heat sink to a typical cryo pulse-tube cooler with 1 W of cooling power at 4 K by carefully choosing the trap substrate with high heat conductivity (e.g. sapphire) and trap mounting materials.

To further reduce the temperature of the cooling and readout tank circuit substantially below 4 K, a dilution refrigerator can be employed to separately cool the top layer of the trap housing these elements to 40 mK, as shown Fig. 4. In this case, the bottom layer at 4 K, now acts as a heat load on the top layer. The conduction from the 4K layer to the 40 mK layer needs to be low enough to ensure the heat load is lower than the maximum cooling power of the 40 mK stage ($\approx 700\,\mu W$).

To minimize the heat flux between the stages, an appropriate material for the spacers separating the two substrates must be chosen. The spacers need to be good thermal and electrical insulators at cryogenic temperatures. With four cylindrical spacers made of high-pressure fiberglass laminate (G-10) with a diameter of 1 mm and a length of 2 mm, the heat load on the top layer of the trap is $\approx 500\,\mu W$, which is within the cooling capacity of a commercial dilution refrigerator with a minimum cooling power of $\approx 700\,\mu W$.

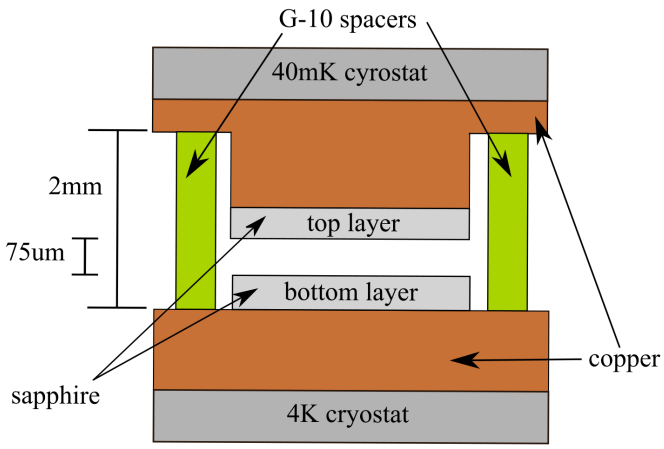


Figure 4: Schematic of advanced version of electron trap with a 4K cryostat and a dilution fridge which cools the top layer to 40 mK substrate. The two substrates are separated by G-10 spacers.

# B Strong drive in motion detection

The amplifiers needed to detect the electron signal are prone to saturation due to the strong AC-drive of the electron trap. To estimate the degree of filtering necessary to successfully detect an electron in the presence of the 10 GHz drive, we model the electron as a Johnson-noise source with a bandwidth of 1 MHz at 4 K corresponding to a noise power of -132 dBm, where the bandwidth is determined by the coupling of the electron to the tank circuit. Assuming a dynamic range of the amplifier of 70 dB, the pick up at the drive frequency at $\sim 10$ GHz must be smaller than -60 dBm. We estimate that the power required to drive the trap will be of order 1 W (30 dBm) requiring an effective filtering of 90 dBm.

First, we note that the resonant circuit picking up the signal from the electron itself serves as a filter: the trap drive is many GHz detuned from the resonant circuits narrow resonance $\Delta\omega$ at $\omega_r = 2\pi \times 2$ GHz. Secondly, the amplifier itself will be optimized to amplify the 2 GHz signal rather than the high frequency drive. Further, we plan to pick up the image current from electrodes in the top substrate in Fig. 1 rather than in the bottom substrate thereby rejecting most of the voltage in the first place. Finally, we can filter the signal of $\sim$2 GHz, either via low pass filter, or if that is still not sufficient with another resonant circuit.

# C Quantum gate simulation

The Bell-state fidelity is defined as

$$\mathcal{F} = \langle \Psi_{\text{target}} | \, \rho_{\text{exp}} \, | \Psi_{\text{target}} \rangle \tag{5}$$

where $|\Psi_{\text{target}}\rangle$ is the targeted Bell-state and $\rho_{\text{exp}} = \text{Tr}_{\text{m}}(\rho_T)$ is the reduced density matrix of total system $\rho_T$ tracing out the motional degree of freedom. The gate error is defined as $1 - \mathcal{F}$.

Gate dynamics are simulated with the Lindblad master equation using QuTip [**johansson2012**]:

$$\dot{\rho}(t) = -\frac{i}{\hbar}[H, \rho] + \sum_n \left[ L_n \rho L_n^\dagger - \frac{1}{2}\rho L_n^\dagger L_n - \frac{1}{2} L_n^\dagger L_n \rho \right] \tag{6}$$

where $L_n$ is the Lindblad operator, $\hat{H} = \hat{H}_g + \hat{H}_e$ is the total Hamiltonian consisting of the gate dynamics $\hat{H}_g$ and possible error sources described by $\hat{H}_e$.

The gate Hamiltonian is described as:

$$\hat{H}_g = \hbar\Omega_R(\hat{I} \otimes \hat{\sigma}_z + \hat{\sigma}_z \otimes \hat{I})(\hat{a}e^{-i\delta t} + \hat{a}^\dagger e^{i\delta t}) \tag{7}$$

**Motional heating:** Motional heating is modeled with the Lindblad operators $L_n = \sqrt{\gamma}\hat{a}$,$\sqrt{\gamma}\hat{a}^\dagger$, where $\gamma = \dot{n}_e$ is the motional heating rate, $\hat{a}^\dagger$ and $\hat{a}$ are the creation and annihilation operator of the motional mode, respectively.

**Motional frequency fluctuation:** Motional frequency fluctuations are modeled with the Hamiltonian

$$\hat{H}_e = \hbar\Delta\hat{a}^\dagger\hat{a} \tag{8}$$

where $\Delta$ is the motional frequency detuning from $\omega_a$.

**Motional dephasing:** Motional dephasing is modeled with the Lindblad operator $L_n = \sqrt{\Gamma}\hat{a}^\dagger\hat{a}$, where $\Gamma$ is the dephasing rate of the electron motion.

**Inhomogeneity of the magnetic field gradient:** Taylor expanding the magnetic field gradient at electron location $\nabla B = B^{(1)} + B^{(2)}\delta z + \frac{1}{2}B^{(3)}\delta z^2$, the magnetic field gradient inhomogeneity error is modeled with the Hamiltonian:

$$\hat{H}_e = \hbar\Omega_{\text{in}}(\hat{I} \otimes \hat{\sigma}_z + \hat{\sigma}_z \otimes \hat{I})(2\hat{a}_j^\dagger\hat{a}_j + 1)(\hat{a}e^{-i\delta t} + \hat{a}^\dagger e^{i\delta t}) \tag{9}$$

where $\Omega_{in} = \Omega_R \cdot \frac{j_0^2}{2}\frac{B^{(3)}}{B^{(1)}}$, $j_0$ is the ground state extension of motional mode $j$, and $B^{(i)}$ is the $i-th$ order derivative of the magnetic field.

**Anharmonicity of the potentials:** Expanding the trapping potential to only the fourth order $V(z) = V(0)(1 + c_2z^2 + c_4z^4)$, the trap potential anharmonicity can be modeled with the Hamiltonian

$$\hat{H}_e = V_4\hat{z}^4 = V(0)c_4z_0^4(\hat{a}_z + \hat{a}_z^\dagger)^4 \tag{10}$$

**Qubit decoherence:** Qubit decoherence is modeled with the Lindblad operator $L_n = \sqrt{\frac{1}{2\tau_{\text{spin}}}}\hat{\sigma}_z$, where $\tau_{\text{spin}}$ is the spin coherence time.

# D Electron trajectory stability

The electron trajectory stability is analyzed by numerically integrating the electron motion along radial directions. The simulation variables are the phase of the AC drive at the ionization time and the initial energy of electrons in the AC trapping potential which is determined by the ionization distance from the trap center. Fig. 5 shows the simulation result, which is a map of the electron storage time simulated up to 100 µs. From the simulation, electron trajectories are stable for initial energies less than 60 K which corresponds to an ionization distance of about 4 µm from the trap center. For higher energies, the stability of the electron trajectory will depend strongly on the phase of the AC drive, and electron trajectories are the most stable when initially the relative phase between the electron secular motion and the AC drive is zero.

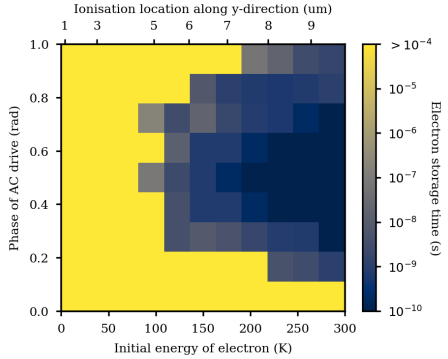


Figure 5: Electron trajectory simulation of two-dimensional secular motion. Electron trajectories are universally stable for initial energies less than 60 K and are the most stable with in phase AC drive.

# References


[1] Natalie C. Brown and Kenneth R. Brown. "Comparing Zeeman qubits to hyperfine qubits in the context of the surface code: 174Yb+ and 171Yb+". In: *Physical Review A* 97.5 (May 2018), p. 052301. DOI: 10.1103/PhysRevA.97.052301.

[2] Nikos Daniilidis, Dylan J Gorman, Lin Tian, and Häffner Hartmut. "Quantum information processing with trapped electrons and superconducting electronics". In: *New J. Phys.* 15 (2013), p. 073017. DOI: 10.1088/1367-2630/15/7/073017.

[3] P. Peng, C. Matthiesen, and H. Häffner. "Spin readout of trapped electron qubits". In: *Physical Review A* 95.1 (Jan. 2017), p. 012312. DOI: 10.1103/PhysRevA.95.012312.

[4] Shlomi Kotler, Raymond W. Simmonds, Dietrich Leibfried, and David J. Wineland. "Hybrid quantum systems with trapped charged particles". In: *Physical Review A* 95.2 (Feb. 2017), p. 022327. DOI: 10.1103/PhysRevA.95.022327.

[5] Clemens Matthiesen, Qian Yu, Jinen Guo, Alberto M. Alonso, and Hartmut Häffner. "Trapping Electrons in a Room-Temperature Microwave Paul Trap". In: *Physical Review X* 11.1 (Jan. 2021), p. 11019. DOI: 10.1103/physrevx.11.011019.

[6] D J Wineland and H G Dehmelt. "Principles of the stored ion calorimeter". In: *J. App. Phys.* 46 (1975), p. 919. DOI: 10.1063/1.321602.

[7] L.S. S S S Brown and G. Gabrielse. "Geonium theory: Physics of a single electron or ion in a Penning trap". In: *Reviews of Modern Physics* 58.1 (1986), pp. 233–311. DOI: 10.1103/RevModPhys.58.233.

[8] Dylan J Gorman, Philipp Schindler, Sankaranarayanan Selvarajan, Nikos Daniilidis, and Hartmut Häffner. "Two-mode coupling in a single-ion oscillator via parametric resonance". In: *Physical Review A* 89.6 (June 2014), p. 062332. DOI: 10.1103/PhysRevA.89.062332.

[9] S. C. Burd, R. Srinivas, J. J. Bollinger, A. C. Wilson, D. J. Wineland, D. Leibfried, D. H. Slichter, and D. T.C. Allcock. "Quantum amplification of mechanical oscillator motion". In: *Science* 364.6446 (2019), pp. 1163–1165. DOI: 10.1126/science.aaw2884.

[10] S. C. Burd, R. Srinivas, H. M. Knaack, W. Ge, A. C. Wilson, D. J. Wineland, D. Leibfried, J. J. Bollinger, D. T.C. Allcock, and D. H. Slichter. "Quantum amplification of boson-mediated interactions". In: *Nature Physics* (May 2021), pp. 1–5. DOI: 10.1038/s41567-021-01237-9.

[11] David J Wineland, P Ekstrom, and Hans Dehmelt. "Monoelectron Oscillator". In: *Physical Review Letters* 31.21 (1973), pp. 1279–1282.

[12] Eric A. Cornell, Robert M. Weisskoff, Kevin R. Boyce, and David E. Pritchard. "Mode coupling in a Penning trap: {¡}i{¿}$π${¡}/i{¿} pulses and a classical avoided crossing". In: *Physical Review A* 41.1 (Jan. 1990), pp. 312–315. DOI: 10.1103/PhysRevA.41.312.

[13] Sven Sturm, Anke Wagner, Birgit Schabinger, and Klaus Blaum. "Phase-Sensitive Cyclotron Frequency Measurements at Ultralow Energies". In: *Physical Review Letters* 107.14 (Sept. 2011), p. 143003. DOI: 10.1103/PhysRevLett.107.143003.

[14] T. P. Harty, D. T. C. Allcock, C. J. Ballance, L. Guidoni, H. A. Janacek, N. M. Linke, D. N. Stacey, and D. M. Lucas. "High-Fidelity Preparation, Gates, Memory, and Readout of a Trapped-Ion Quantum Bit". In: *Physical Review Letters* 113.22 (Nov. 2014), p. 220501. DOI: 10.1103/PhysRevLett.113.220501.

[15] Klaus Mølmer and Anders S Sørensen. "Multiparticle entanglement of hot trapped ions." In: *Phys. Rev. Lett.* 82 (1999), p. 1835. DOI: https://doi.org/10.1103/PhysRevLett.82.1971.

[16] Christian F Roos. "Ion trap quantum gates with amplitude-modulated laser beams". In: *New Journal of Physics* 10.1 (Jan. 2008), p. 013002. DOI: 10.1088/1367-2630/10/1/013002.

[17] D Leibfried et al. "Experimental demonstration of a robust, high-fidelity geometric two ion-qubit phase gate". In: *Nature* 422 (2003), pp. 412–415. DOI: 10.1038/nature01492.

[18] C. Ospelkaus, U. Warring, Y. Colombe, K. R. Brown, J. M. Amini, D. Leibfried, and D. J. Wineland. "Microwave quantum logic gates for trapped ions". In: *Nature* 476.7359 (Aug. 2011), pp. 181–184. DOI: 10.1038/nature10290.

[19] F. Mintert and C. Wunderlich. "Ion-trap quantum logic using long-wavelength radiation." In: *Physical Review Letters* 87 (2001), p. 257904. DOI: 10.1103/PhysRevLett.87.257904.

[20] C. Ospelkaus, C. E Langer, J. M Amini, K. R Brown, D. Leibfried, and D. J Wineland. "Trapped-Ion Quantum Logic Gates Based on Oscillating Magnetic Fields". In: *Physical Review Letters* 101.9 (Aug. 2008), p. 90502. DOI: 10.1103/PhysRevLett.101.090502.

[21] R. Srinivas, S. C. Burd, R. T. Sutherland, A. C. Wilson, D. J. Wineland, D. Leibfried, D. T. C. Allcock, and D. H. Slichter. "Trapped-ion spin-motion coupling with microwaves and a near-motional oscillating magnetic field gradient". In: *arXiv:1812.02098 [quant-ph]* (Dec. 2018).

[22] T. P. P. Harty, M. A. A. Sepiol, D. T. C. T. C. Allcock, C. J. J. Ballance, J. E. E. Tarlton, and D. M. M. Lucas. "High-Fidelity Trapped-Ion Quantum Logic Using Near-Field Microwaves". In: *Physical Review Letters* 117.14 (Sept. 2016), p. 140501. DOI: 10.1103/PhysRevLett.117.140501.

[23] R Srinivas et al. "High-fidelity laser-free universal control of two trapped ion qubits". In: *arXiv:2102.12533v1 [quant-ph]* (2021).

[24] Tom Manovitz, Amit Rotem, Ravid Shaniv, Itsik Cohen, Yotam Shapira, Nitzan Akerman, Alex Retzker, and Roee Ozeri. "Fast Dynamical Decoupling of the Mølmer-Sørensen Entangling Gate". In: *Physical Review Letters* 119.22 (Nov. 2017), p. 220505. DOI: 10.1103/PhysRevLett.119.220505.

[25] A E Webb, S C Webster, S Collingbourne, D Bretaud, A M Lawrence, S Weidt, F Mintert, and W K Hensinger. "Resilient Entangling Gates for Trapped Ions". In: *Phys. Rev. Lett.* 121 (2018), p. 180501. DOI: 10.1103/PhysRevLett.121.180501.

[26] R. T. Sutherland, R. Srinivas, S. C. Burd, D. Leibfried, A. C. Wilson, D. J. Wineland, D. T.C. Allcock, D. H. Slichter, and S. B. Libby. "Versatile laser-free trapped-ion entangling gates". In: *New Journal of Physics* 21.3 (Mar. 2019), p. 33033. DOI: 10.1088/1367-2630/ab0be5.

[27] RT Sutherland, Raghavendra Srinivas, Shaun C Burd, Hannah M Knaack, Andrew C Wilson, David J Wineland, Dietrich Leibfried, DTC Allcock, Daniel H Slichter, and SB Libby. "Laser-free trapped-ion entangling gates with simultaneous insensitivity to qubit and motional decoherence". In: *Phys. Rev. A* 101.4 (2020), p. 042334.

[28] M. Brownnutt, M. Kumph, P. Rabl, and R. Blatt. "Ion-trap measurements of electric-field noise near surfaces". In: *Reviews of Modern Physics* 87.4 (Dec. 2015), pp. 1419–1482. DOI: 10.1103/RevModPhys.87.1419.

[29] Kenneth R. Brown, John Chiaverini, Jeremy Sage, and Hartmut Häffner. "Materials Challenges for Trapped-Ion Quantum Computers". In: *arXiv: 2009.00568 [quant-ph]* (Sept. 2020).

[30] D. A. Hite et al. "100-Fold Reduction of Electric-Field Noise in an Ion Trap Cleaned with In Situ Argon-Ion-Beam Bombardment". In: *Physical Review Letters* 109.10 (Sept. 2012), p. 103001. DOI: 10.1103/PhysRevLett.109.103001.

[31] J. A. Sedlacek, J. Stuart, D. H. Slichter, C. D. Bruzewicz, R. McConnell, J. M. Sage, and J. Chiaverini. "Evidence for multiple mechanisms underlying surface electric-field noise in ion traps". In: *Physical Review A* 98.6 (Dec. 2018), p. 63430. DOI: 10.1103/PhysRevA.98.063430.

[32] Crystal Noel, Maya Berlin-Udi, Clemens Matthiesen, Jessica Yu, Yi Zhou, Vincenzo Lordi, and Hartmut Häffner. "Electric-field noise from thermally activated fluctuators in a surface ion trap". In: *Physical Review A* 99.6 (June 2019), p. 063427. DOI: 10.1103/PhysRevA.99.063427.

[33] David Hayes, Susan M Clark, Shantanu Debnath, David Hucul, I Volkan Inlek, Kenny W Lee, Qudsia Quraishi, and Christopher Monroe. "Coherent error suppression in multiqubit entangling gates". In: *Physical review letters* 109.2 (2012), p. 020503.

[34] Farhang Haddadfarshi and Florian Mintert. "High fidelity quantum gates of trapped ions in the presence of motional heating". In: *New Journal of Physics* 18.12 (Dec. 2016), p. 123007. DOI: 10.1088/1367-2630/18/12/123007.

[35] Yotam Shapira, Ravid Shaniv, Tom Manovitz, Nitzan Akerman, and Roee Ozeri. "Robust Entanglement Gates for Trapped-Ion Qubits". In: *Physical Review Letters* 121.18 (2018), p. 180502. DOI: 10.1103/PhysRevLett.121.180502.

[36] I. Talukdar, D. J. Gorman, N. Daniilidis, P. Schindler, S. Ebadi, H. Kaufmann, T. Zhang, and H. Häffner. "Implications of surface noise for the motional coherence of trapped ions". In: *Physical Review A* 93.4 (Apr. 2016), p. 043415. DOI: 10.1103/PhysRevA.93.043415.

[37] T. Ruster, C. T. Schmiegelow, H. Kaufmann, C. Warschburger, F. Schmidt-Kaler, and U. G. Poschinger. "A long-lived Zeeman trapped-ion qubit". In: *Applied Physics B* 122.10 (Oct. 2016), p. 254. DOI: 10.1007/s00340-016-6527-4.

[38] D Kielpinski, C Monroe, and D J Wineland. "Architecture for a large-scale ion-trap quantum computer." In: *Nature* 417.6890 (2002), pp. 709–711. DOI: 10.1038/nature00784.

[39] B. Lekitsch, S. Weidt, A. G. Fowler, K. Mølmer, S. J. Devitt, C. Wunderlich, and W. K. Hensinger. "Blueprint for a microwave trapped ion quantum computer". In: *Science Advances* 3.2 (Feb. 2017), e1601540. DOI: 10.1126/sciadv.1601540.

[40] R. Bowler, J. Gaebler, Y. Lin, T. R. Tan, D. Hanneke, J. D. Jost, J. P. Home, D. Leibfried, and D. J. Wineland. "Coherent Diabatic Ion Transport and Separation in a Multizone Trap Array". In: *Physical Review Letters* 109.8 (Aug. 2012), p. 080502. DOI: 10.1103/PhysRevLett.109.080502.

[41] H Kaufmann, T Ruster, C T Schmiegelow, F Schmidt-Kaler, and U G Poschinger. "Dynamics and control of fast ion crystal splitting in segmented Paul traps". In: *New Journal of Physics* 16.7 (July 2014), p. 073012. DOI: 10.1088/1367-2630/16/7/073012.

[42] D Hucul, I V Inlek, G Vittorini, C Crocker, S Debnath, S M Clark, and C Monroe. "Modular entanglement of atomic qubits using photons and phonons". In: *NATURE PHYSICS* — 11 (2015). DOI: 10.1038/NPHYS3150.

[43] L J Stephenson, D P Nadlinger, B C Nichol, S An, P Drmota, T G Ballance, K Thirumalai, J F Goodwin, D M Lucas, and C J Ballance. "High-rate, high-fidelity entanglement of qubits across an elementary quantum network". In: *arXiv: 1911.10841 [quant-ph]* (2020).

[44] David P DiVincenzo. "The physical implementation of quantum computation". In: *Fortschritte der Physik: Progress of Physics* 48.9-11 (2000), pp. 771–783.

[45] J. R. Danielson, D. H.E. Dubin, R. G. Greaves, and C. M. Surko. "Plasma and trap-based techniques for science with positrons". In: *Reviews of Modern Physics* 87.1 (Mar. 2015), pp. 247–306. DOI: 10.1103/RevModPhys.87.247.

[46] William P. Putnam and Mehmet Fatih Yanik. "Noninvasive electron microscopy with interaction-free quantum measurements". In: *Phys. Rev. A* 80 (4 Oct. 2009), p. 040902. DOI: 10.1103/PhysRevA.80.040902.

[47] Daniel Carney, Hartmut Häffner, David C. Moore, and Jacob M. Taylor. *Trapped electrons and ions as particle detectors*. 2021. arXiv: 2104.05737 [quant-ph].

[48] Nathan Leefer, Kai Krimmel, William Bertsche, Dmitry Budker, Joel Fajans, Ron Folman, Hartmut Häffner, and Ferdinand Schmidt-Kaler. "Investigation of two-frequency Paul traps for antihydrogen production". In: *Hyperfine Interactions* 238.1 (2016), p. 12. DOI: 10.1007/s10751-016-1388-0.